

Article

Fatigue Analysis of a Longitudinally Oriented Ellipsoidal Crack in the ERW of ASTM A53 Type E Gr B Carbon Steel Pipe in a Lithium Process Plant

Luis Espinoza *, Jose Antonio Bea

Department of Mechanical Engineering, University of Zaragoza, Zaragoza 50009, Spain

* Correspondence: 846552@unizar.es

Received: 15 April 2025; Accepted: 21 July 2025; Published: 15 August 2025

Abstract: The main goal of this approach is to present a technical analysis based on fracture mechanics theory, examining the fatigue behaviour of a simulated longitudinal crack with an ellipsoidal geometry in a firewater pipeline belonging to a process plant designed under the ASME B31.3 Process Piping Design Code for processing lithium ore in northern Argentina. The study focuses on a straight section of carbon steel piping (ASTM A53 Type E Gr B) with a diameter of 20 inches, simulating a longitudinal crack with an ellipsoidal base induced in the upper part of the forging area. This is under pressure design conditions of ± 1.30 MPa (σ_m Mean Stress = 0) and a constant temperature of 60 °C, according to the design specifications of the lithium extraction project A1C. This approach uses the strain-life fatigue analysis method available in the Ansys fatigue module. Strain-life is usually concerned with crack initiation. This procedure uses a numerical simulation method in the ANSYS 2025 R1 workbench. The results show that the lowest fatigue life occurs in the FWZ (Forged Weld Zone) area of the ERW. Once the obtained values have been analysed, the critical zones of the crack and low cycling are identified. It is suggested that pressure should be kept below the critical value, and that experimental studies available in literature should be carried out to compare the results of this approach. These conclusions form the basis for applied research in real case studies in industry.

Keywords: mechanical fatigue; carbon steel; electric resistance welding (ERW); finite element method (FEM); lithium process plant

Nomenclature

a	Crack Depth
ANSYS	Stand For Analysis System
A1C	Design Specification for firefighting water
ASTM	American Standard Testing Material
A53	Grades of steel according to ASTM
API	American Petroleum Institute
APIX65	Material Grade X65
APIX70	Material Grade X70
ASME	American Standard Mechanical Engineer
BM	Base Metal
°C	Degrees Celsius
da/dN	Crack Growth Rate

DWG	Drawing Extension AutoCAD
ERW	Electrical Resistance Welding
e	Young's modulus
FEM	Finite Element Method
FWZ	Forged Weld Zone
FD	Fatigue Damage
GTAW	Gas Tungsten Arc Welding
HAZ	Heat Affected Zone
In	Inches
LIF	Life in Fatigue
MPa	Megapascal Unit of pressure
OD	Outside Diameter
ID	Inside Diameter
PD	Desing pressure
P	Pressure applied
PA	Pascal
R_i	Internal Radio
R_e	External Radio
T_s	Thickness
STD	Schedulle Standard of Piping
SPEC	Specification of Piping Class
SIF	Stress Intensity Factor
SF	Safety Factor
SMAW	Shielded Metal Arc Welding
SSWC	Selective Seam Weld Corrosion
SEM	Scanning Electron Microscope
SCH	Schedulle
.sat	Extension of file to import from Cad to ANSYS
TD	Design Temperature
USGS	U.S. Geological Survey
ν	Poisson's ratio/coefficient
WTa	Wall Thickness failed before
WTb	Wall Thickness after failed
X, Y, Z	Axis
σ_m	Mean Stress
$\Delta\epsilon/2$	Total strain Amplitude
σ_f	Fatigue Strength Coefficient
$2N_f$	Number of reversals to Failure
N_f	Number of Cycle to Failure

1. Introduction

According to the USGS Mineral Commodity Summaries [1], lithium resources totalling approximately 20 million tonnes have been detected in Argentina, surpassing countries such as China, Australia, Chile, Canada and Mexico. Since 1991, Minera Altiplano S.A., an American subsidiary of Livent Corp [2], has operated in the north of Argentina, with an estimated production of 20,000 tons.

Phase I, the SA plant process design, is based on existing Livent technology. The plant feed is fresh brine with a lithium concentration of 600 ppm [3] Pre-concentration of brine in solar ponds is included in the project. The process plant will be built according to specifications developed using the American National Standard Code for Pressure Piping Process Piping (ASME B31.3) [4]. This code is usually used for many piping systems in the erection of process plants. One of the most important units in this plant is the fire water station, where the 20-inch-diameter carbon steel piping (ASTM A53 Type E Gr B) shows a crack of an ellipsoidal base induced in the upper part of the ERW forging area.

In industrial environments, we are usually surrounded by several pipes, both underground and above ground, which supply different services. These pipes are often joined by ERW types, which have been found to have several cracks that have caused accidents. This study focuses on the fatigue behaviour of API-X70 steel [5].

According to Krupp Ulrich's proposal regarding fatigue crack propagation in metals and alloys, the study of fatigue behaviour in materials has been ongoing for at least 150 years [6]. This is of great importance in an industrial context worldwide, and studies of mechanical elements yielding significant advances in crack prediction will continue to be conducted, as emphasised by renowned scholars in this field, such as Paris and Paul [7]. However, fatigue crack growth is an even more complex process involving load cycling, and better analysis in this area is needed.

On the other hand, FEM (Finite Element Method), a numerical technique for finding approximate solutions in engineering, provides an important scope and contribution to the field of engineering problem solving. Problems are mostly identified by presenting differential equations, boundary conditions and geometries [8].

Zilong Xia et al. analysed a leakage in a buried fire water pipeline that occurred after 15 years in service. The pipeline was manufactured from a Q235B carbon structural steel plate using high-frequency electric resistance welding. They conducted their analysis using a combination of experimental metallography and theoretical finite element modelling with Ansys software. The pipeline operated within a pressure range of 0.8 to 1.2 MPa. Following experimental and theoretical analysis, the results showed that the main cause of cracking in the pipe was low heat input and that selective weld seam corrosion (SSWC) also had a significant effect [9].

Brian Young et al. made approximations using fatigue models that had been applied to the cracking of ERW welds in pipelines for the estimation of mechanical fatigue crack growth. These approximations were made in an experimental setting using X-70, X-52 and B grade steels [10,11]. Their results showed that the threshold model can characterize the stress intensity range as a function of material grade and stress ratio, and that this method can be used to estimate crack growth rates. The aim of this study is to reduce accidents in pipe networks with a high rate of weld failure.

Zhang Guangli et al. carried out an experimental study on the fatigue characteristics of an ERW weld on an API X65 pipeline material, as well as evaluating the fatigue life. Their main finding was that the main cause of cracks in ERW pipes is cold welding, and they provided technical

support for this in the form of the API 579-2007 standard, also known as the failure assessment diagram [12].

Zilong Xia et al., have elaborated a paper concerning an analysis of an ERW weld in a fire water pipeline belonging to a chemical plant. The crack is located at the bottom of the pipe. They have developed a macro morphology and metallographic analysis using a scanning electron microscope (SEM), as well as finite element method (FEM) simulations. The numerical and experimental results summarized that insufficient fusion of heat and selective seam weld corrosion (SSWC) contributed to the formation and progression of cracking. For this reason, when high pressure is produced in the pipe network, plus the effect of SSWC, cracking will be present. The crack location and the macro morphology of the pipeline at the leak and the affected weld zones are shown in Figure 1 [13].

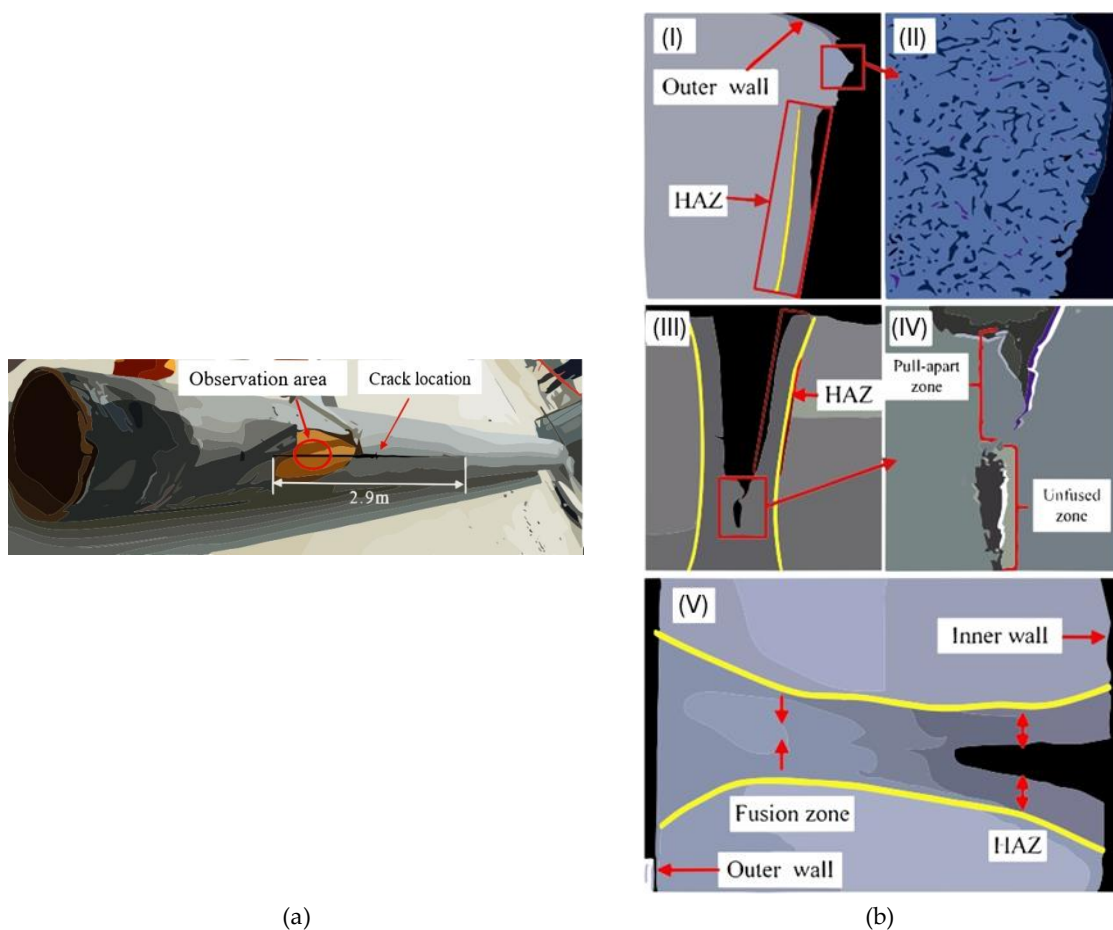


Figure 1. (a) Crack at the weld of pipeline. (b) The weld zones affected.

In 2023, Gang Wang et al. analysed the fatigue behaviour of a circumferential crack in a pipe using numerical analysis. They used a reinforced polymer fibre to validate and evaluate the fatigue life and stress intensity factor (SIF). This pipe belongs to marine engineering plants. The following Figure 2 shows the crack characteristics [14].

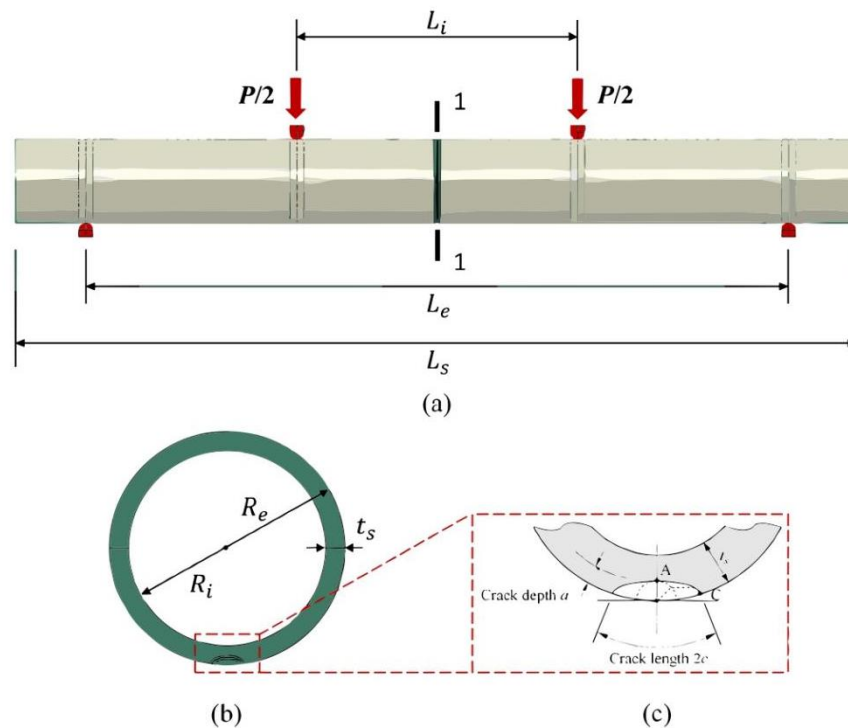


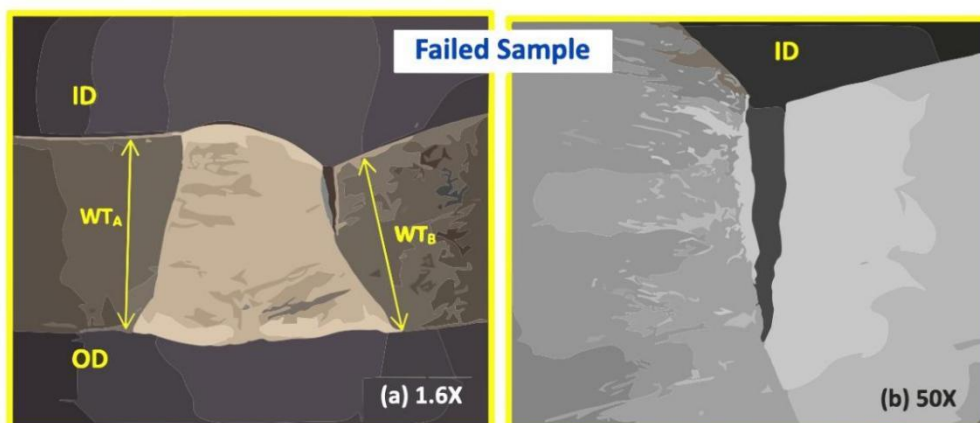
Figure 2. (a) Geometry of unrepaired steel pipe, (b) elevation of specimen and (c) crack details.

Their results showed that the initial size of cracks has an impact on the fatigue behaviour of steel pipes, particularly with regard to the SIF. The design of the polymer fibre reinforcement contributed to reducing the rate of crack propagation.

Recently, Gazala Mohamed et al. analysed several factors influencing the failure of a seam-welded pipeline under the action of fatigue and thermal conditions. Their study covered a SS 304L pipeline, using experimental analysis and numerical simulations with FEM. Figure 3 shows the crack (failed sample) and a 3D representation of the crack. Figure 4 shows a mesh scheme and a zoom of the crack tip.

Their findings revealed that the main cause of the failure was the residual stresses in the HAZ, with two important issues to consider: The welding sub-procedures and their post-treatment [15].

This approach will contribute to the exploration of a real industrial case in a firewater station with piping designed to international standards. This station belongs to a lithium plant located in the north of Argentina. The approach uses the advantages offered by FEM with ANSYS Workbench and the Fatigue Module, which represent a versatile technical tool based on scientific theory and engineering experience.



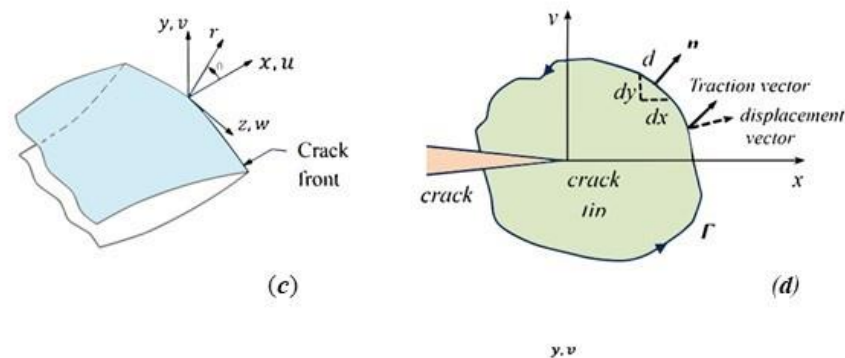


Figure 3. (a, b) Failed sample of crack base metal. (c, d) Local coordinate system and contour at the crack tip.

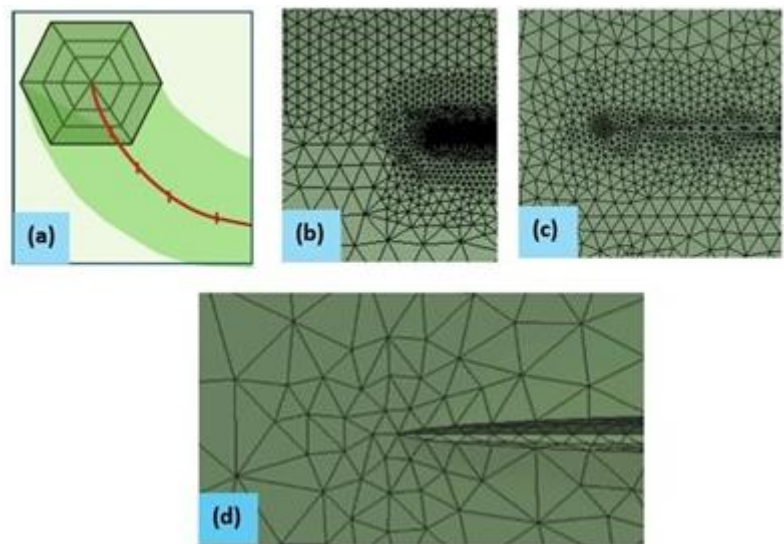


Figure 4. (a) Schematic of mesh generation. (b, c) zoom at the crack tip, (d) More zoom showing mesh contour.

The main goal of this proposal is to offer an easy way to solve industrial problems that arise in the daily operations of installations. These installations have human and environmental responsibilities and must implement policies to guarantee optimal performance.

The pipeline design is under SPEC A1C (Figure 5) which shows the following values:

PIPE CLASS	A1C					
SERVICE:	COMPRESSED AIR (AC1), FILTERED RAW WATER (WA1, WR1) FILTERED WATER (WU1), FIREWATER (WF2)					
MATERIAL:	Carbon Steel					
RATING CLASS:	150, ASME B16.5	DESIGN CODE:		ASME B31.3		
		STRESS RELIEF:		Per ASME B31.3		
NOMINAL CORROSION ALLOWANCE:	1.5 mm	EXAMINATION:		Per ASME B31.3		
PRESSURE - TEMPERATURE RATINGS 10 BARG AT 60 DEGC						
ITEM	NOTE	NPS	SCH/RAT	ENDS	DESCRIPTION	USER CODE
PIPE		1/2 - 2	80		CS, ERW, ASTM A53 TYPE E, GR B, T&C, GALV	
		2-1/2 - 10	40		CS, ERW, ASTM A53 TYPE E GR B	
		12 - 24	STD		CS, ERW, ASTM A53 TYPE E GR B	

Figure 5. Spec A1C

The main zones in the weld where fatigue damage is greatest will be identified, as will the fatigue life and safety factor. The cycles at which these concepts will be reached in the fatigue study will be estimated, and the sensitivity graph will be commented on.

2. Method and Material

Figure 6 below presents the methodology applied in this approach in a very general way [16].

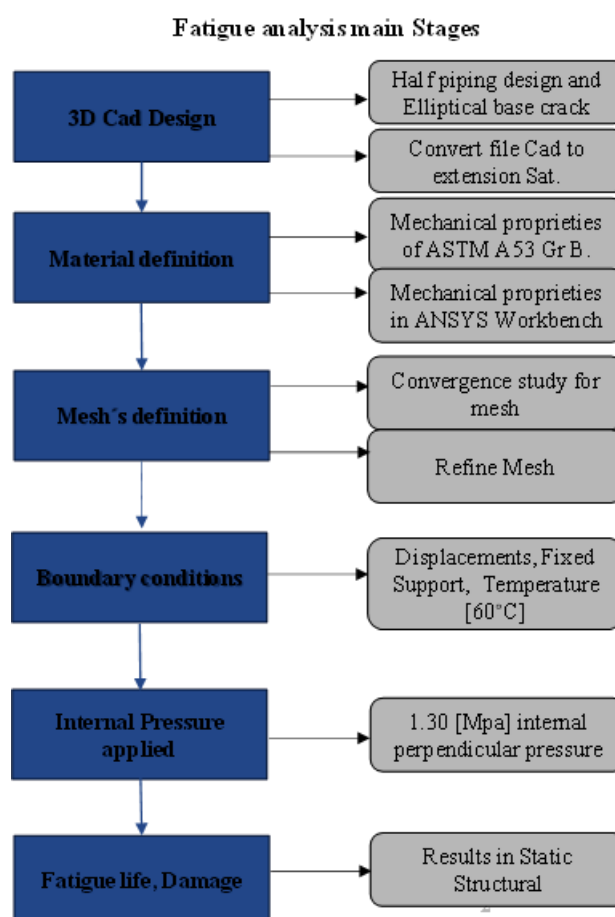


Figure 6. Step-by-step diagram of study.

2.1 Auto CAD 3D Design (Model and Location of the Crack)

The geometry consisted of a straight pipe (cylinder) with a diameter of 20 inches, a thickness of 0.375 inches and a length of 6 metres. It was manufactured in the workshop for use in the field. A longitudinal crack with an elliptical cross-section and ellipsoidal ends was designed symmetrically and modelled. Only half of the pipe was used to ensure computational savings, given that the simulation was performed using an academic licence. Figure 7 shows half of the 20-inch pipe (Importing a CAD model into FEM software, for example, reduces the effort of producing a geometric model with all its lines, circles, surfaces and so on [17]).

The geometry was designed in a DWG file, which is then converted to a '.sat' extension before being imported into the Ansys Workbench module to check for any import warnings. The dimensions of the longitudinal crack are: The crack is 0.4 mm wide and 1 mm high, and its depth (a) is 6.56 mm. See Figure 8.

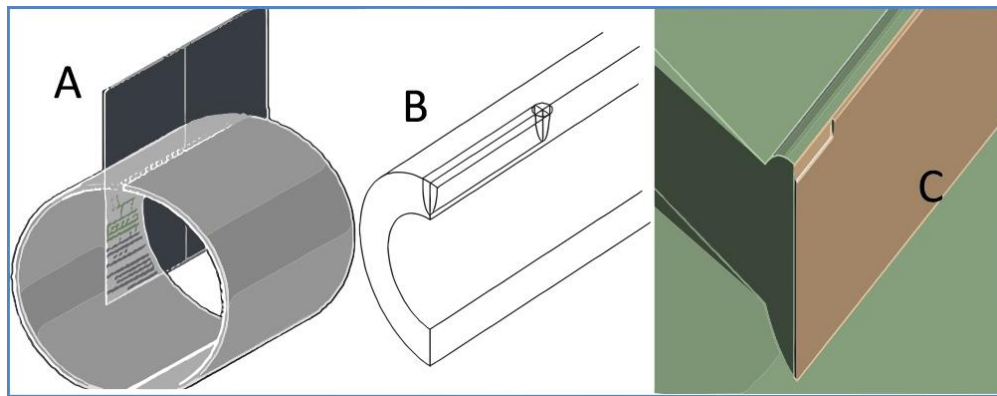


Figure 7. Geometry of 20-inch pipe with ellipsoidal crack. (A) Complete pipe under ASME B36.10. and cutting plane. (B) Half pipe with ellipsoidal base crack. (C) Import of "sat" file in ANSYS.

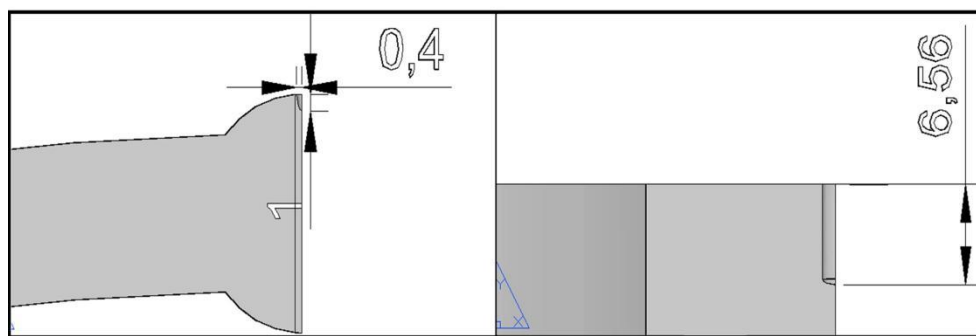


Figure 8. Approach of the longitudinal crack and Depth of the crack (plan view).

2.2 Mechanical Proprieties of Material

For the study, an isotropic material (carbon steel) with a modulus of elasticity of $E = 2 \times 10^{11}$ Pa and a Poisson's ratio of 0.3 was considered. The following table summarizes the most important mechanical properties of the carbon steel (ASTM A53 Gr B [18]) under test, as defined in the "Engineering Data" module of the ANSYS program. See Table 1.

Table 1. Mechanical properties of ASTM A53 Gr B [19].

Mechanical Proprieties	ASTM A53 Grade B
Tensile strength, min, psi [Pa]	60.000 (4.15×10^8)
Yield Strength, min, psi, [Pa]	35.000 (2.40×10^8)
Density	7850 [Kg/m ³]
Coefficient of thermal expansion	1.02×10^{-5}
Young's modulus [e]	2×10^{11} [Pa]
Poisson's radius [v]	0.3
Curve type	Strain-Life

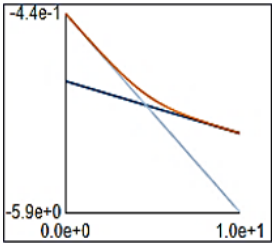
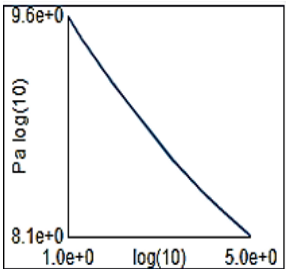
*<https://protoandgo.com/materiales/acero-al-carbono/>

2.3 Mechanical Proprieties in ANSYS Workbench

To guarantee an effective simulation, all the mechanical properties of the pipe material must be declared in Ansys. To do this, enter the data into the matrix space in Workbench Static Structural, ensuring that the units are in the same system. The strain-life method will be applied for fatigue in

this approach (Stress life methods are most useful at high cycle fatigue, where the applied stresses are elastic, and no plastic strain occurs anywhere other than at the tips of fatigue cracks. At low cycles, scatter in the fatigue data makes these methods increasingly less reliable [20]). Table 2 shows the input data for the material used in ANSYS.

Table 2. Mechanical properties of ASTM A53 Gr B material in Ansys. [19, 20, 21, 22, 23].

ASTM A53 Type E Gr B	
Structural: Isotropic Elasticity	
Density	7850 [Kg/m3]
Derive from	Young's Modulus and Poisson's Ratio
Young's Modulus	2e+11 [Pa]
Poisson's Ratio	0.3
Bulk Modulus	1.6667e+11 [Pa]
Shear Modulus	7.6923e+10 [Pa]
Isotropic Secant Coefficient of Thermal Expansion	1.2 e-0.5 1/°C
Compressive Ultimate Strength	0 [Pa]
Compressive Yield Strength	2.4e+14 [Pa]
Strain-Life Parameters	
S-N Curve	
Tensile Ultimate Strength	4.15e+08 [Pa]
Tensile Yield Strength	2.4 e+08 [Pa]

2.4 Converge Study for Mesh

To ensure the analysis is accurate, it is necessary to estimate how small the element should be for the mesh solution to be trustworthy [16]. The convergence of the meshing should not produce significant numerical differences; this variable is of the utmost importance when capturing stress peaks or deformations [24].

The version of ANSYS Academic used has limits on the number of nodes and elements. In this case, the existing capacity was tested by iterating and estimating the equivalent stress (von Mises) [25], as shown in Table 3 below.

Table 3. Iterations for converge mesh example.

Iteration	"Mesh Resolution"	Number of elements at HAZ	Equivalent Stress (Max) (Von Mises) [Pa]	Variation Between Iteration
1	1	349	1,09E+09	
2	2	231	1,09E+09	0%
3	3	451	1,11E+09	1.47%
4	4	910	1,15E+09	3.66%
5	5	1474	1,11E+10	960.39%
6	6	2912	4,46E+09	40.33%

The results of the iterations indicated that there is no variation between #1 and #2, as shown in the following chart (Figure 9).

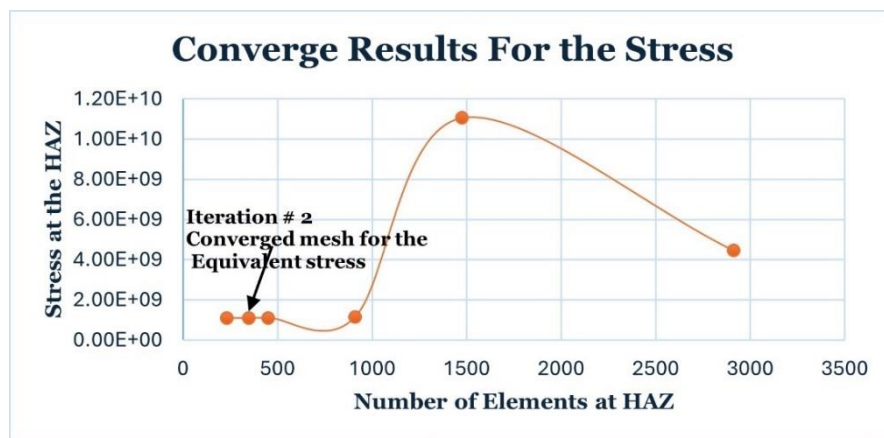


Figure 9. Converge results for Equivalent Stress Von Misses.

According to the convergence results, 231 elements in the HAZ will be used to create the mesh. A level-3 mesh refinement was performed in the area where the weld (HAZ) is located, which is the maximum allowed. See Table 3 and Figure 9.

It should be noted that the refined mesh physically encompasses a significantly larger portion of the domain in the finite-element representation and provides a more accurate representation of the edges of the figure [26]. See Figures 10, 11 and 12.

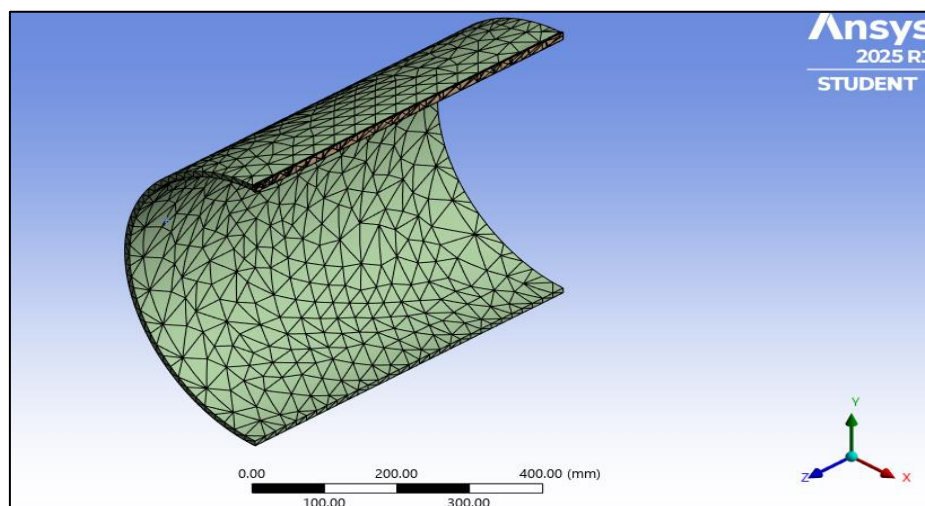


Figure 10. Meshing Model.

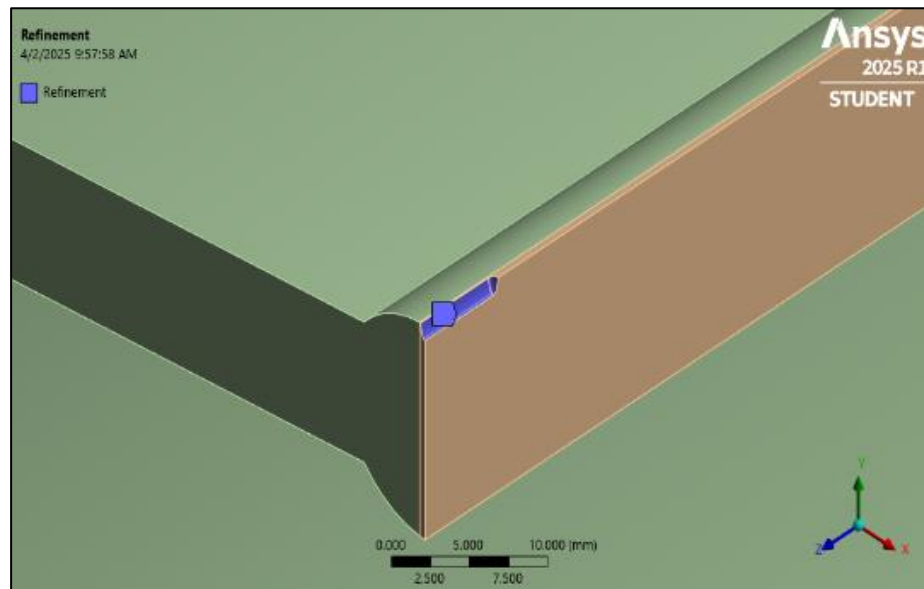


Figure 11. Refinement of Mesh.

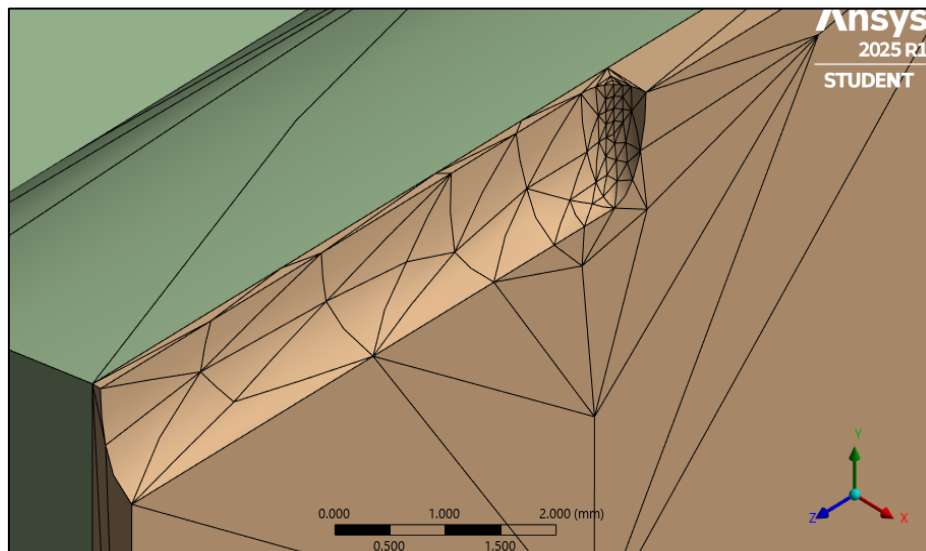


Figure 12. Zoom Refinement of Mesh level 3.

Table 4 below shows the statistics and elements used to build the mesh, taking into account mesh refinement level 3.

Table 4. Statistics and element of meshing.

Statistics of Meshing		Element Order
Nodes	1019	Quadratic (Retains midsize nodes on elements created in the part or body. All elements have midsize nodes.)
Elements	422	

2.5 Boundary Conditions

The following boundary conditions are applied to this model: displacement along the Z-axis and Y-axis, loading, contact with the support, and a fixed support. [27].

The displacements along the Y and Z axes are restricted, i.e. they are considered to be zero.

Loading: An internal pressure of 1.3 MPa is applied perpendicular to the pipe at specific points. This applied pressure is a constant value.

Contact with support: This condition represents the pipe's contact with the supports.

Fixed support: In order to simulate a logical case in the Ansys program, it is necessary to establish a fixed support. This immobilizes a face and avoids movement or deformation in this area. In practice, the pipe is joined to a 6 m long pipe section; this condition therefore represents the joint. Figure 13 summarizes all the boundary conditions considered for the model.

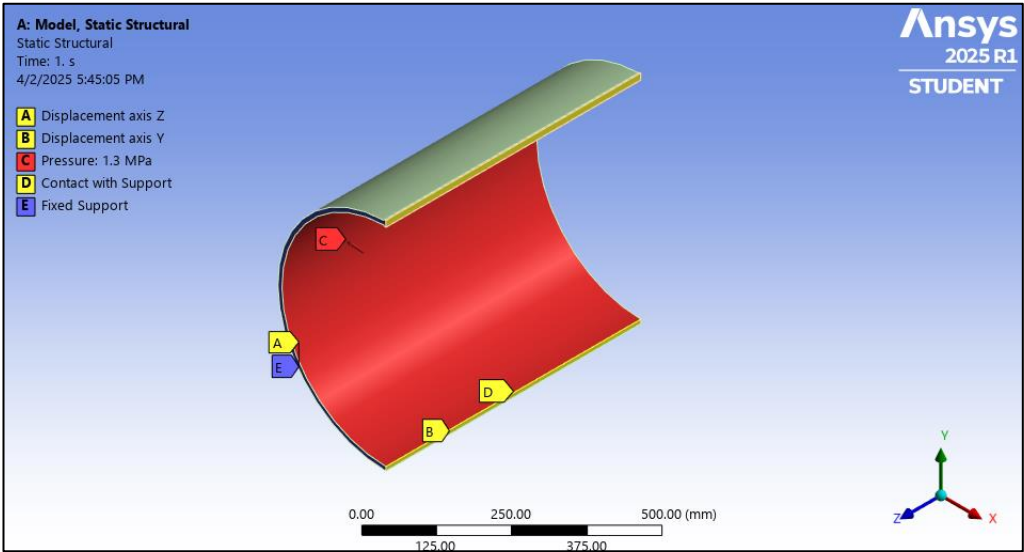


Figure 13. Boundary conditions summary.

2.6. Thermal Condition

Another important condition to consider is the design temperature 60 °C (Design temperature of equipment and piping systems is generally defined as the temperature corresponding to the most severe condition of coincident temperature and pressure to which the system will be subjected [28].), this variable is applied to all the geometry, as a representation of the contact between the water flow and the internal part of the pipe, since the ansys program gives only one option to incorporate this variable, which includes all the geometry both externally and internally. Please see Figure 14.

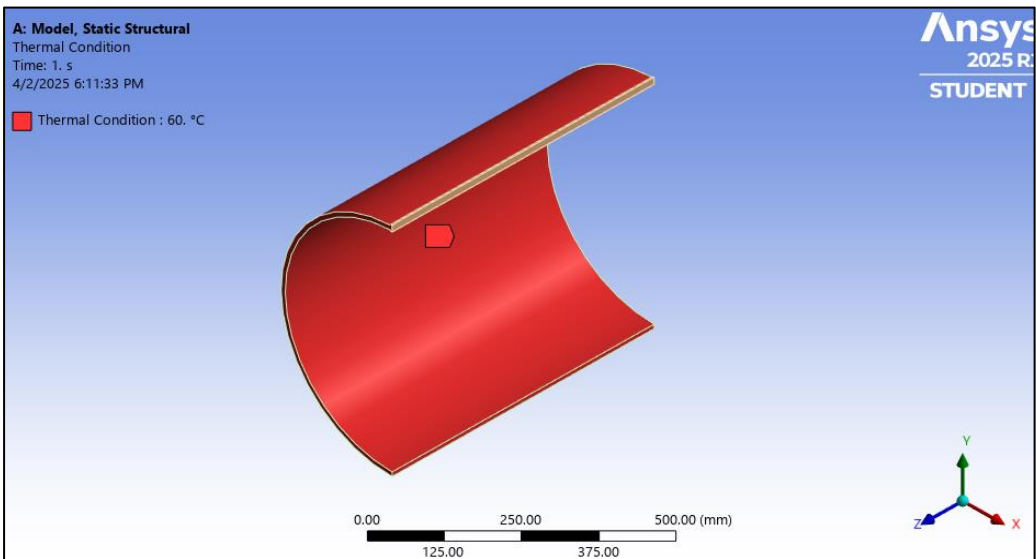


Figure 14. Temperature condition in the middle of the pipe.

The following Table 5 shows a summary of the boundary conditions used in this approach.

Table 5. Summary of the boundary conditions used.

Summary of Boundary Conditions	
Displacement axis Y and Z	Value = 0
Loading	Value = 1.3 [Mpa]
Contact with Support	Value = D (See figure 13)
Fixed Support	Value = E (See figure 13)
Thermal condition	Value = 60 [°C]

This analysis uses the Deformable life method, which is typically employed in low-cycle fatigue scenarios involving a combination of elastic and plastic loading at the macro scale [29].

On the other hand, the constant amplitude-proportional load is of constant amplitude because only one set of stresses results throughout, with a load radius. This is required to calculate the mean and alternative values [30]. For this exercise, the values are considered to have a reversion index of $R = -1.5$, which indicates a tensile-compressive stress of $\sigma = 1.3$, as shown in Figure 15 [31].

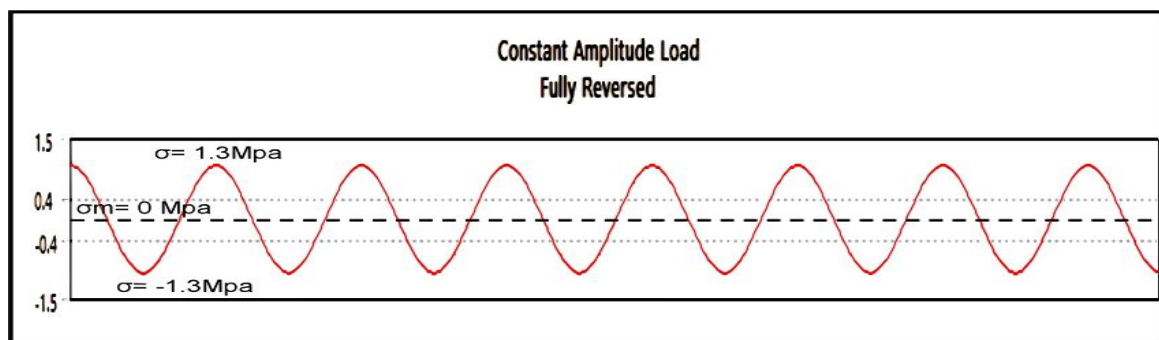


Figure 15. Diagram for constant amplitude loading.

2.7. Governing Equations

This approach uses a strain-life fatigue analysis, which is based on the strain-life relation equation. This equation uses strain-life parameters, which are values for a particular material that best fit the equation to the measured results.

In order to carry out this method, it is essential to define the properties of the ASTM A53 Gr B material. The strain-life relation equation requires a total of six parameters to define the strain-life material properties: Strength Coefficient (1), Strength Exponent (2), Ductility Coefficient (3), Ductility Exponent (4), Cyclic Strength Coefficient (5) and Cyclic Strain Hardening Exponent (6) [32]. See table 6.

The main equation used in the strain-life simulation is presented below.

$$\frac{\Delta \epsilon}{2} = \frac{\sigma_f}{E} (2N_f)^b + \epsilon_f (2N_f)^c \quad (\text{Strain Life}) \quad (2)$$

where:

$$\frac{\Delta \epsilon}{2} = \text{Total Strain Amplitud}$$

$$\sigma_f = \text{Fatigue Strenght Coefficient}$$

$$E = \text{Modulus of Elasticity}$$

$$2N_f = \text{Number of Reversals to Failure}$$

$$N_f = \text{Number of Cycle to Failure}$$

Table 6. Parameters to define the strain-life material properties.

Properties of Outline Row 4: ASTM53 Type E Gr B		
A	B	C
Strain-Life Parameters	Value	Unit
Display Curve Type	Strain-Life	
Strength Coefficient	9.64E+08	[Pa]
Strength Exponent	-0.145	
Ductility Coefficient	0.36	
Ductility Exponent	-0.55	
Cyclic Strength Coefficient	1E+09	[Pa]
Cyclic Strain Hardening Exponent	0.26	

3. Results and Discussion

The following results were obtained using the static structural module of Ansys in the mechanical fatigue option, once the simulations had been carried out with the premises established in the boundary conditions and the engineering data. The contour drawings showing the estimated fatigue life, fatigue damage, factor of safety, equivalent elastic strain and equivalent plastic strain are presented below.

3.1 Life

Once the parameters for the fatigue analysis have been defined and the corresponding iteration performed using the above values, the following results are obtained. The resulting contours show the fatigue life. If the load is of constant amplitude, as in this case, the resulting model represents the number of cycles until the element fails due to fatigue.

The red contour plane in Figure 16a indicates the maximum number of cycles in 1×10^5 (infinite life), which was predetermined for the analysis. However, by zooming in on Figure 16b, it can be seen that the minimum number of cycles occurs in the FWZ (Forged Weld Zone: A weld that results from processes that combine the use of heat and high pressure, or forging forces applied to the weld zone [33]) area, with a value of 56,167 cycles. This value is between 1 and 100 cycles, which Joseph Edward Shigley [34] refers to as 'low cycle fatigue' or 'low cycling'. In other words, once this number of cycles has been reached, this would be the first area to fail (shown in red). The above figures show that the surface towards the base of the crack, extending through the area of the ellipsoidal base weld forging in the pipe belonging to the fire-fighting system, has the lowest fatigue life.

In the area of the weld seam where the crack is present, the following cycles are identified with the colours orange, yellow and light green: 359, 2294.6 and 14666, respectively. See figures 16a and 16b. In summary, the locations of the cracks and their associated cycles are shown in Table 7.

Table 7. Summary of Cycles at Ellipsoidal crack in piping of firefighting.

Crack Location	Low-Cycle fatigue $N < 10^3$ [cycles]	High-Cycle fatigue $N > 10^3$ [cycles]
Base Ellipsoidal	56,167* /359	14666/2294,6/93742
Longitudinal Surface of Forged Weld Zone	56,167* /359	*Minimum cycles

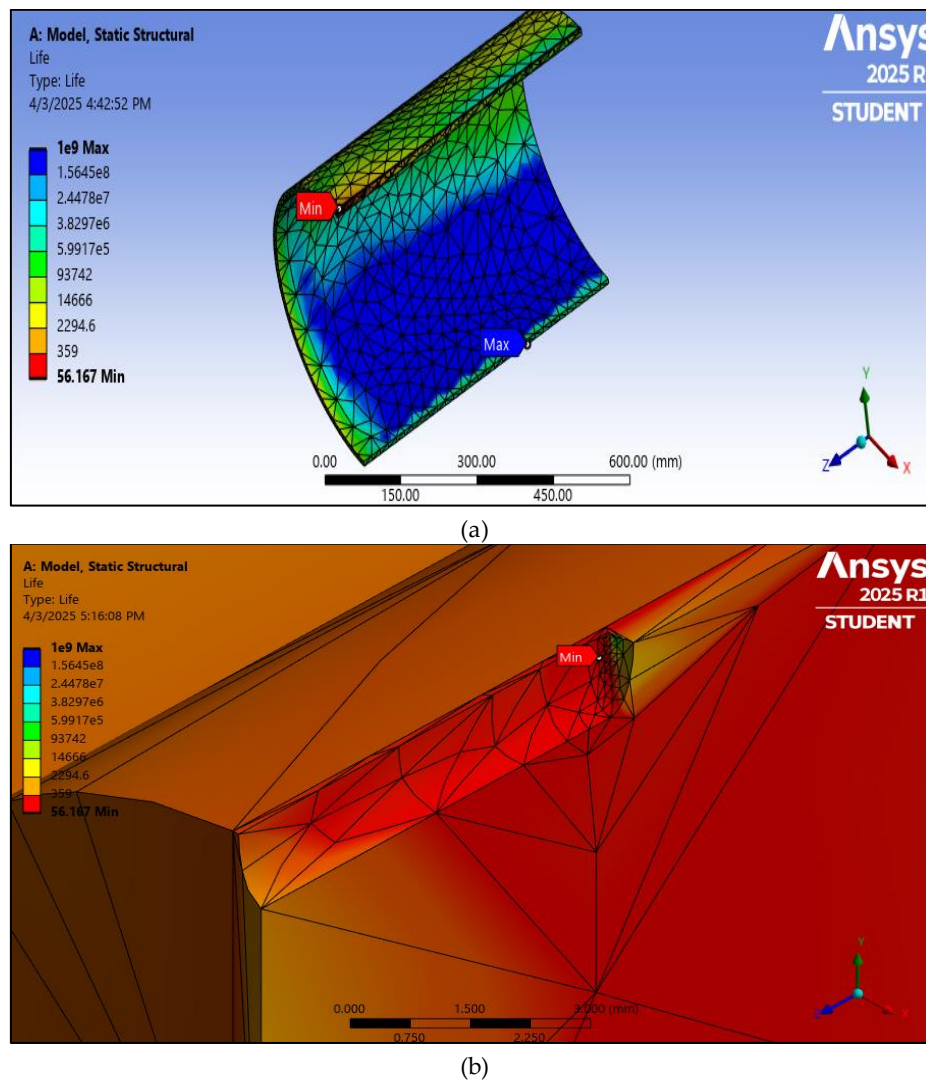


Figure 16. (a) Contour plane life in fatigue of the affected part in the welding seam. (b) Zoom at the first area of fail.

3.2 Damage

This analysis is a contour plane of fatigue damage (In ANSYS, fatigue damage is a measure of how close a material is to failure under cyclic loading. It represents the accumulated degradation of a material subjected to repeated stress or strain. Source: <https://ansyshelp.ansys.com/>), as defined by the strain life method. Values greater than 1 indicate failure before the design life is reached.

Figures 17a and 17b show the damage in the red area towards the FWZ. Zooming in on this area reveals the damage around the induced crack, which has a value of 1. The maximum damage is located at the ellipsoidal base of the induced crack in the FWZ weld zone and has a value of $1,7804 \times 10^7$ cycles.

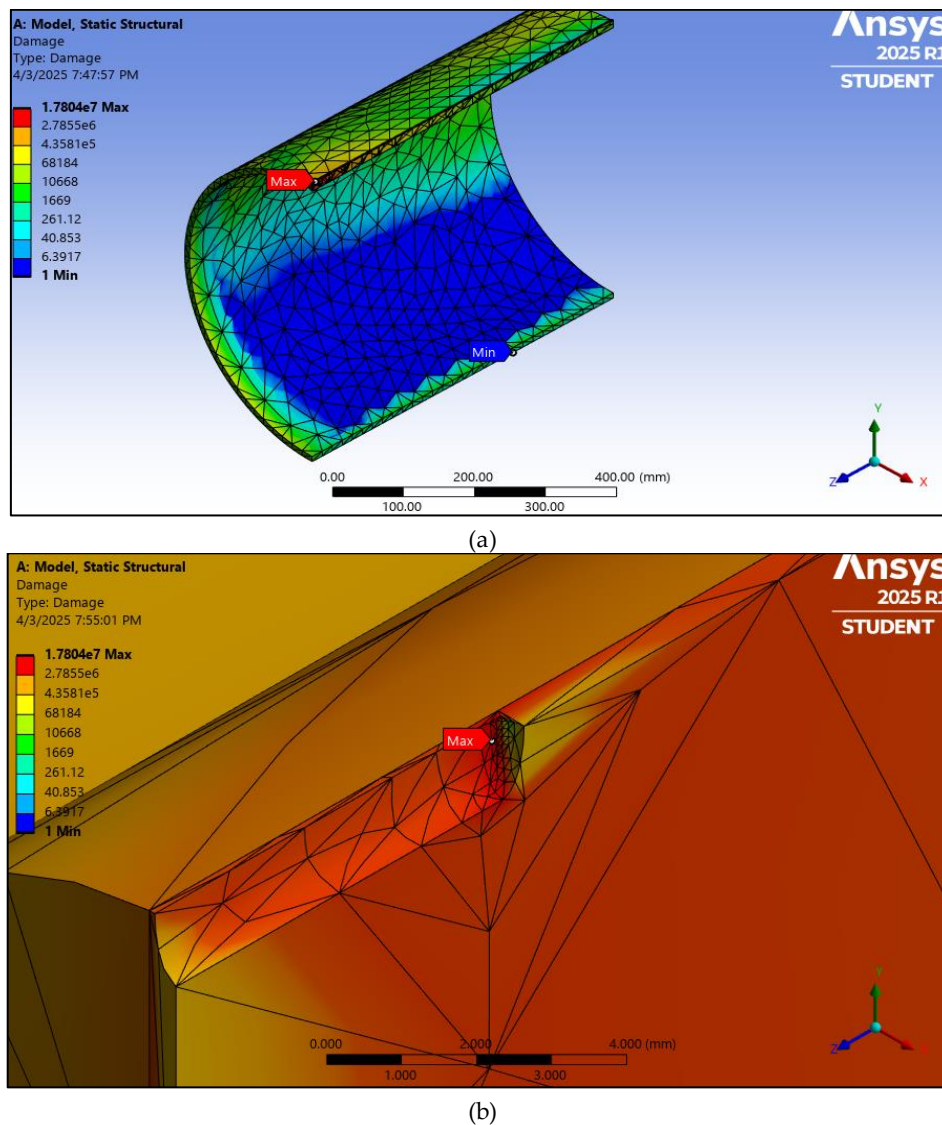


Figure 17. (a) Contour of damage in half piping. (b) Contour drawing for damage in the ERW area.

In summary, Table 8 shows the locations of Max Damage and the associated Cycles.

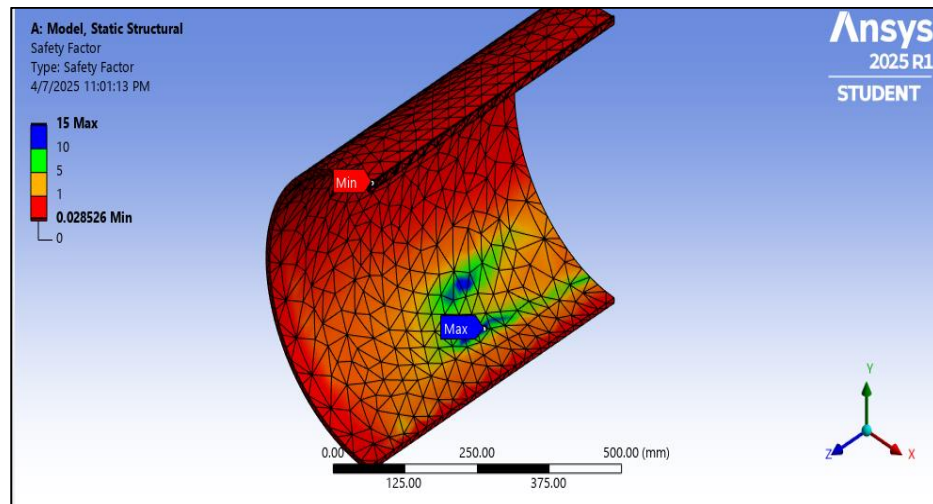
Table 8. Summary of Cycles at Ellipsoidal crack in piping of firefighting. (Damage).

Crack Location	Low-Cycle fatigue $N < 10^3$ [cycles]	High-Cycle fatigue $N > 10^3$ [cycles]
Base Ellipsoidal	None	*14666/2294,6/2,7855e6
Longitudinal Surface of Forged Weld Zone	None	*1,7804e7/2,7855e6
Base Metal	6,39/40,853/261,12	*Max Cycles

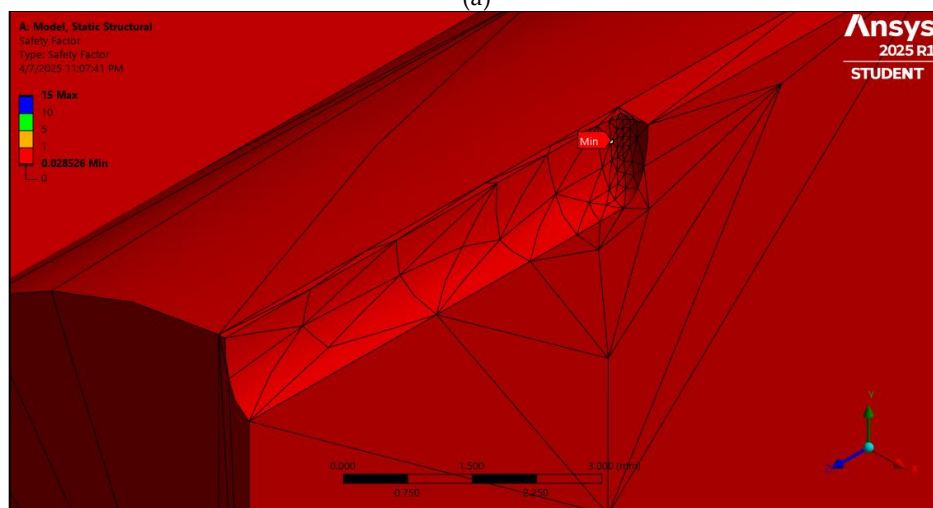
3.3 Safety Factor (SF)

This factor of safety is shown on a contour plane with respect to fatigue failure for a design life of 1×10^9 cycles. The theory is based on the idea that values less than 1 indicate failure before the design life is reached. The maximum safe value is 15.

The area with a value below 1 is the area of the crack base in its ellipsoidal part. This is estimated to be 0.028526. See Figures 18a and 18b.



(a)

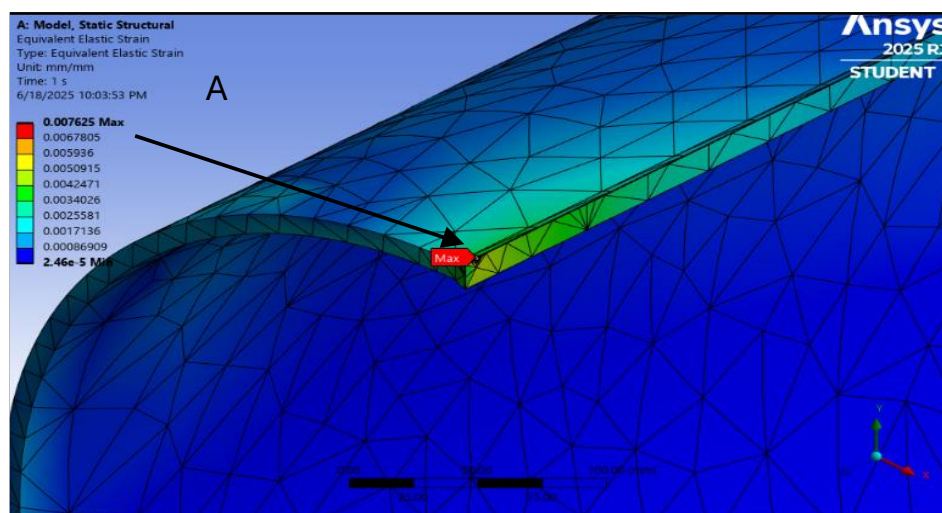


(b)

Figure 18. (a) Fatigue safety factor for life design at half piping. (b) Zoom at the ellipsoidal base.

3.4 Equivalent Elastic Strain

In ANSYS, equivalent elastic deformation is the scalar measure of deformation experienced by the material. Figure 19 below shows the maximum deformation towards the ellipsoidal base of the crack, identified in red, with a value of 0.007625 mm/mm.



(a)

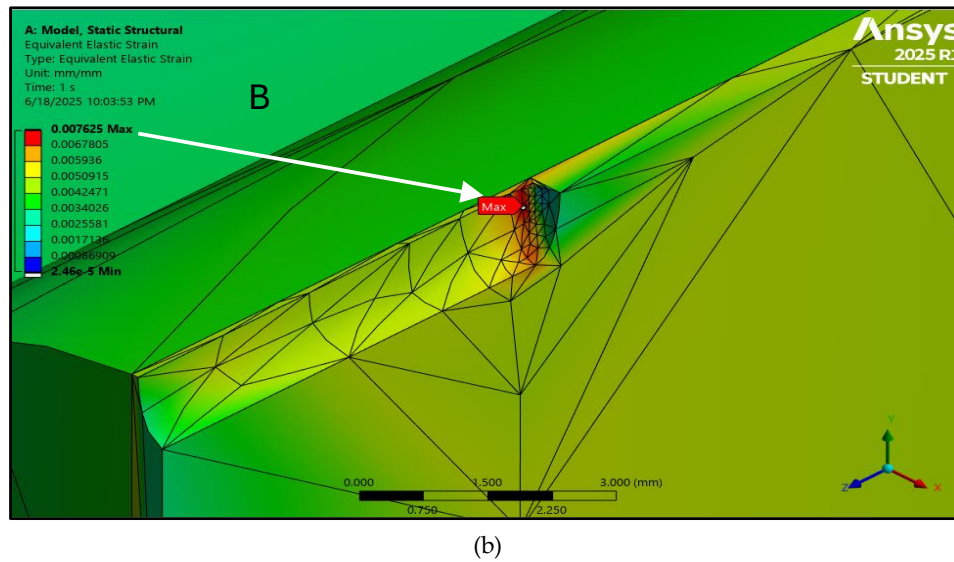


Figure 19. (a) Equivalent Elastic Strain at ERW. (b) Maximum deformation at the ellipsoidal base..

3.5 Equivalent Plastic Strain

The equivalent plastic strain, as defined in ANSYS, is a measure of the total plastic strain experienced by the material, expressed as a single value. In this case, our approximation shows that there is no plastic strain [35]; in other words, the crack has not yet reached the point of rupture. See Figure 20 below.

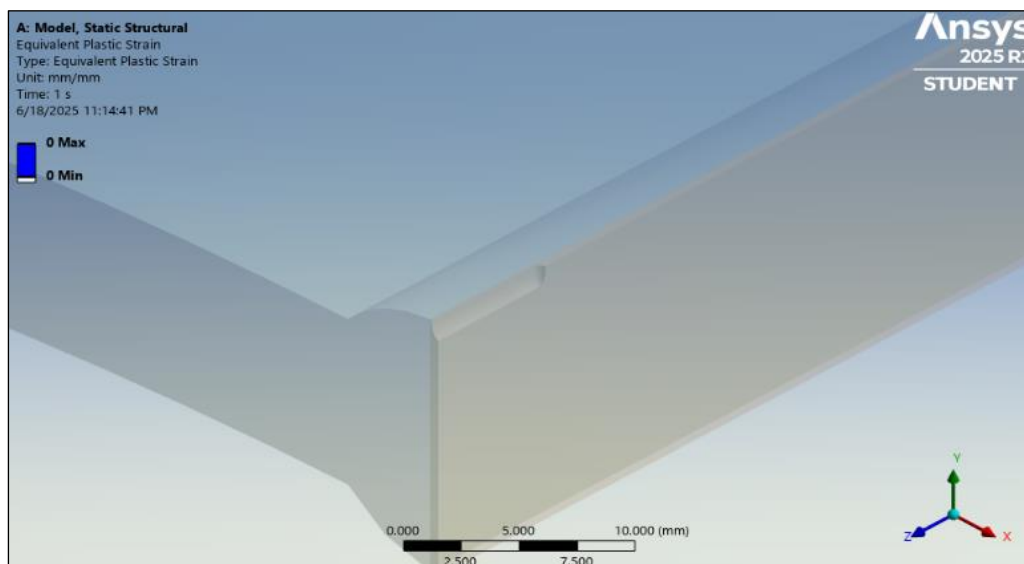


Figure 20. Equivalent Plastic Strain at ERW.

This value indicates that the tensile strength of ASTM A53 Grade B material (4.15×10^8 PA) is not met, as shown in Table 2. The mechanical properties of ASTM A53 Gr B are presented in this research.

This fatigue analysis of the longitudinal ellipsoidal base crack in the ERW of the ASTM A53 Type E Gr. carbon steel pipe belonging to a lithium processing plant was performed using FEM, followed by mesh refinement at the crack tip.

The results can be found in the following Table 9 [16, 36].

Table 9. Summary of results.

Summary of results				
Life [Cycles]	Damage [Cycles]	Safety Factor	Equivalent Elastic Strain [mm/mm]	Equivalent Plastic Strain [mm/mm]
Elements	422	422	0.007625	0

4. Discussion of Limitations

The final mesh model was created for a cracked carbon steel weld. A more refined mesh could improve the model, but this would require the most time-consuming step in the pre-processing workflow. The simulations were performed using an academic ANSYS licence, which restricts the number of nodal partitions.

The lowest fatigue life occurs in the FWZ (Forged Weld Zone) area of the ERW, towards the section where the ellipsoidal base of the crack is. The Longitudinal Surface of the Forged Weld Zone is considered to be low cycle fatigue, with values between approximately 1 and 100 cycles. According to the contour plane, there is an area of the FWZ where the fatigue life would be reached by at least 56,167 cycles.

The maximum initial damage is located at the ellipsoidal base of the crack in length, but according to Figure 18a and 18b, it varies between 1.7804e7 and 2.7855e6 cycles.

Similarly, the estimated minimum safety factor of 0.028526, identified in red in Figures 19a and 19b, is shown by the FEM analysis using the design life. This value is found in the entire ERW weld towards the ellipsoidal base.

A comparison of the number of cycles at the metal base (MB) and the heat-affected zone (HAZ) shows a higher number of cycles for the HAZ. In the case of fatigue life, our results are compared with an experimental analysis called 'Fatigue tests on circumferential welds of X60 steel used for gas pipes'. After the specimens have been pre-cracked and fatigued, the crack will grow in both the base metal and the weld fusion zone due to the higher number of accumulated cycles. However, the steel under test has a higher yield strength. For example, specimen S5 reached 37,086 cycles in the experiment, whereas our numerical results were 56,167. See Table 10 below [37].

Table 10. Shows the number of pre-cracking cycles for each specimen tested.

Number of pre-cracking cycles on base metal specimens [B1-B2] and welded joint specimens [S1-S5]				
B1	B2	B3	B4	B5
15140	28494	20831	27948	26566
S1	S2	S3	S4	S5
30293	32046	34434	36229	37086

As quoted by Mgonja, this fire water pipeline of the lithium plant is prone to failure as long as it is subjected to stress. "Cracks have a tendency to propagate and can contribute to weld failure if subjected to stress in service", but it must be checked in situ.[38].

From the literature reviewed, there was no evidence of a fracture case with the exact characteristics presented in this test. However, surface quality, toughness and stress concentration are considered factors that can affect the fatigue behaviour of a longitudinal weld, as detailed by P. Simon et al. in their experimental study of the fatigue behaviour of longitudinal welded pipes.[39].

5. Conclusions and Recommendations

In this approach, the fatigue analysis of a longitudinally oriented ellipsoidal crack at the ERW of an ASTM A53 Type E Gr B pipe belonging to a lithium process plant was investigated numerically. The FEM model was constructed according to the methodology of a real case study from the lithium process plant. The main conclusions can be summarised as follows:

- The lowest fatigue life occurs in the FWZ (Forged Weld Zone) area of the ERW weld, towards the section where the ellipsoidal base of the crack is located. This is considered to be low cycle fatigue ($N < 10^3$ cycles), with values ranging from approximately 1 to 359 cycles. The initial damage is also located at the ellipsoidal base of the crack.
- The fatigue damage is concentrated along the entire length of the weld, particularly towards the ellipsoidal base metal ($N < 10^3$ cycles).
- According to the results obtained for the safety factor, the lowest value is found in the area of the crack and part of the base metal. This is why it is suggested that the operation of the line be kept to a minimum or that the section of pipe where the crack is being replaced, as well as some type of analysis being suggested, such as: Stress corrosion cracking, hydrogen-induced cracking and welding procedure.
- This study is unique in terms of the specific load conditions, the crack modelling approach, and the implications for lithium plant operations. A future study comparing alternative welding techniques (e.g. GTAW and SMAW) or materials (e.g. API X65 and X70) would be interesting and could provide new insights.
- In view of the results of the fatigue analysis for this specific case, the following is recommended:
 - a) Maintain the lowest possible flow through that line, compensating with the other existing fire system lines, and take monthly load measurements, updating the fatigue damage contours.
 - b) Perform a hot repair of the weld bead.
 - c) Implement a replacement plan for the 6-inch pipe and associated welds that complies with minimum quality requirements to guarantee better performance.
- As with any numerical method, this research provides an approximate solution, so it is recommended that it is verified experimentally. It is intended as a base reference for future research on mechanical fatigue crack growth in different ERW pipelines in process plant stations, combined cycle plants, oil and gas upgrading plants, and energy plants.

Data availability: Data will be made available on request.

Author Contributions: Conceptualization, L.E. and J.A.B.; methodology, L.E.; software, L.E. and J.A.B.; Validation, L.E.; formal analysis, L.E.; investigation, L.E.; writing original draft preparation, L.E.; writing—review and editing, L.E. and J.A.B.; visualization, L.E. and J.A.B.; supervision, J.A.B.

Conflicts of Interest: The authors declare no conflict of interest.

References

1. U.S. Geological Survey. Mineral Commodity Summaries 2023. Available online: <https://pubs.usgs.gov/publication/mcs2023> (accessed on 15 April 2025).

2. Barberón, A. El litio en Argentina: Impacto productivo y políticas científico-tecnológicas. *Ciencia, tecnología y política* **2022**, *5*, 81, <https://doi.org/10.24215/26183188e081>.
3. Livent corporations. Process Design Basis. SK-P-1222-02. Rev F1, Pages 3-10, 2020 .
4. Livent corporations. Piping material specification. 24110-8230-SP-0002. Rev F3, pages 2-3, 2020.
5. Hong, H.U.; Kim, C.M.; Lee, J.B. Fatigue behavior of electric resistance welded seams in API-X70 steel. Proceedings of the 15th (2005) International Offshore and Polar Engineering Conference, Seoul, Korea, June 19-24, 2005.
6. Krupp, U. Fatigue crack propagation in metals and alloys: microstructural aspects and modelling concepts. John Wiley & Sons: Hoboken, NJ, USA.
7. Paris, P.C. A brief history of the crack tip stress intensity factor and its application. *Meccanica* **2014**, *49*, 759-764, <https://doi.org/10.1007/s11012-014-9896-y>.
8. Dechaumphai, P.; Sucharitpwatskul, S. *Finite element analysis with ANSYS workbench*. Alpha Science International Limited: Oxford, England, 2018.
9. Xia, Z.; Huang, Y.; Zhong, J.; Guan, K. Cracking failure analysis on a high-frequency electric resistance welding pipe in buried fire water pipeline. *Eng. Fail. Anal.* **2023**, *146*, 107072, <https://doi.org/10.1016/j.engfailanal.2023.107072>.
10. Young, B.A.; Olson, R.J.; O'Brian, J.M. Validation of Fatigue Models for ERW Seam Weld Cracking. In Proceedings of ASME 2017 Pressure Vessels and Piping Conference, Waikoloa, HI, USA, July 16–20, 2017, <https://doi.org/10.1115/PVP2017-65378>.
11. Beavers, J.A.; Brossia, C.S.; Denzine, R.A. Development of Selective Seam Weld Corrosion Test Method. In Proceedings of 2014 10th International Pipeline Conference, Calgary, AB, Canada, September 29–October 3, 2014, <https://doi.org/10.1115/IPC2014-33562>.
12. Zhang, G.; Luo, J.; Zhao, X.; Zhang, H.; Zhang, L.; Zhang, Y. Research on the fatigue character of ERW pipe welded seam and fatigue life assessment method. In Proceedings of 2010 8th International Pipeline Conference, Calgary, AB, Canada, September 27 – October 1, 2010, <https://doi.org/10.1115/IPC2010-31226>.
13. Xia, Z.; Huang, Y.; Zhong, J.; Guan, K. Cracking failure analysis on a high-frequency electric resistance welding pipe in buried fire water pipeline. *Eng. Fail. Anal.* **2023**, *146*, 107072, <https://doi.org/10.1016/j.engfailanal.2023.107072>.
14. Wang, G.; Li, Z.; Chen, T.; Peng, P.; Xiao, Z. Numerical study on fatigue behavior and strengthening of steel pipes with a surface crack. *Theor. Appl. Fract. Mec.* **2023**, *127*, 104003, <https://doi.org/10.1016/j.tafmec.2023.104003>.
15. Gadala, M.; Gadala, I.; Gomaa, A. Failure assessment of seam-welded pipe under fatigue and thermal loading. *Eng. Fail. Anal.* **2025**, *167*, 108934, <https://doi.org/10.1016/j.engfailanal.2024.108934>.
16. Espinoza, L.; Bea, J.A.; Chakraborty, S.; Galatro, D. Comparison of the stress intensity factor for a longitudinal crack in an elliptical base gas pipe, using FEM vs. DCT methods. *Forces Mech.* **2023**, *13*, 100233, <https://doi.org/10.1016/j.finmec.2023.100233>.
17. American Society of Mechanical Engineers. Welded and Seamless Wrought Steel Pipe: ASME B36. 10m. Available online: <https://www.asme.org> (accessed on 17 April 2025).
18. Dechaumphai, P.; Sucharitpwatskul, S. *Finite element analysis with ANSYS workbench*. Alpha Science International Limited.: Oxford, UK, 2018.
19. A53/A53M-20. Standard Specification for Pipe Specification for Pipe, Steel, Black and hot-Dipped. Zinc-Coated. Welded and Seamless. Pag 3. Available online: <https://store.astm.org> (accessed on 15 April 2025).
20. Brush, M. Stress life vs Strain Life. Technical Tidbits. Available online: <https://es.scribd.com> (accessed on 10 March 2025).
21. The Engineering Tool Book. Available online: <https://www.engineeringtoolbox.com/> (accessed on 5 March 2025).
22. WorldAutoSteel. Strength Coefficient. 2024. Available online: <https://www.worldautosteel.org/> (accessed on 10 March 2025).
23. Hernández, I.R.E. Análisis por elemento finito del crecimiento de grieta por fatiga en la soldadura longitudinal erw de una tubería api 5l gr b de acero al carbono. Master dissertation, Universidad Nacional Experimental Politécnica Antonio José de Sucre: Caracas, Venezuela, 2015.
24. Madier, D. *Practical finite element analysis for mechanical engineers*. 2020, Vol. 147, FEA Academy: Montreal, Canada.

25. Goncalves, R. *Introduction to stress analysis*. 2nd ed. 2002, Industrial Grafica Integral C.A: Caracas, Venezuela.
26. Hutton, D. *Fundamentals of finite element analysis*. 2004, McGraw Hill Companies: New York, NY, USA.
27. Boundary conditions. Available online: <https://ansyshelp.ansys.com> (accessed on 2 March 2025).
28. PDVSA. MDP-01-DP-01. *Design Temperature and Pressure*. 1995. PDVSA: Caracas, Venezuela.
29. LibreTexts Physics. Expansion Thermal Iron or steel. (Internet). 2024. Available online: <https://phys.libretexts.org> (accessed on 2 March 2025).
30. Browell, B.R. *Predicting Fatigue Life with ANSYS Workbench*. 2006. Ansys, inc.: Canonsburg, Pennsylvania.
31. Hancq A.D. Fatigue analysis Using Ansys. Pages 2-4. May 2003. Available online: <https://www.ansys.com> (accessed on 15 June 2025).
32. Ansys Help. Available online: <https://ansyshelp.ansys.com> (accessed on 8 April 2025).
33. Metal Fabricating Glossary. Available online: www.thefabricator.com/glossary/forged-weld. (accessed on 15 April 2025)
34. Shigley, J.E.; Mitchell, L.D. *Mechanical Engineering Design* (4th Ed.). *J. Mech. Trans. Automation* **1985**, *107*, 145, <https://doi.org/10.1115/1.3258702>.
35. Ansys. Evaluating Strain Results. Mechanical Strain in Deformation Analysis – lesson 5. Available online: <https://ansyshelp.ansys.com> (accessed on 18 June 2025).
36. Banks-Sills, L.; Sherman, D. Comparison of methods for calculating stress intensity factors with quarter-point elements. *Int. J. Fract.* **1986**, *32*, 127-140, <https://doi.org/10.1007/BF00019788>.
37. Montero, I.; Carboneras, M.; Suárez, J. Ensayos de fatiga en soldaduras circunferenciales de un acero X60 empleado para gasoductos. *Revista española de mecánica de la fractura* **2024**, *7*, 255-260.
38. Mgonja, C.T. The consequences of cracks formed on the oil and gas pipelines weld joints. *Int. J. Eng. Trends Technol.* **2017**, *54*, 223-232, <https://doi.org/10.14445/22315381/IJETT-V54P232>.
39. Simion, P.; Dia, V.; Istrate, B.; Hrituleac, G.; Hrituleac, I.; Munteanu, C. Study of fatigue behavior of longitudinal welded pipes. In 2016 IOP Conference Series: Materials Science and Engineering, Taichung, Taiwan, November 8-11, 2016, <https://doi.org/10.1088/1757-899X/145/2/022032>.



© 2025 by the authors. Submitted for possible open access publication under the terms and conditions of the Creative Commons Attribution (CC BY) license (<http://creativecommons.org/licenses/by/4.0/>).